IEEE Access
Multidisciplinary | Rapid Review | Open Access Journal

Received April 9, 2021, accepted April 25, 2021, date of publication April 28, 2021, date of current version May 19, 2021.

Digital Object Identifier 10.1109/ACCESS.2021.3076308

Passivity Guaranteed Dynamic Friction Model With Temperature and Load Correction: Modeling and Compensation for Collaborative Industrial Robot

MESERET ABAYEBAS TADESE[1,2], FRANCISCO YUMBLA[1,3], (Student Member, IEEE), JUNE-SUP YI[1], WOONGYONG LEE[4], JONGHOON PARK[4], (Member, IEEE), AND HYUNGPIL MOON[5], (Member, IEEE)

[1]Department of Mechanical Engineering, Sungkyunkwan University, Suwon 16419, Republic of Korea
[2]School of Electrical and Computer Engineering, Addis Ababa Institute of Technology, Addis Ababa University, Addis Ababa 385, Ethiopia
[3]Faculty of Mechanical and Production Sciences Engineering, ESPOL Polytechnic University, Guayaquil 09-01-5863, Ecuador
[4]Neuromeka, Seoul 06023, South Korea
[5]Faculty of Mechanical Engineering, Sungkyunkwan University, Suwon 16419, Republic of Korea

Corresponding author: Hyungpil Moon (hyungpil@g.skku.edu)

This work was supported by the Technology Innovation Program or Industrial Strategic Technology Development Program (Development of manipulation technologies in social contexts for human-care service robots) by the Ministry of Trade, Industry & Energy (MOTIE), South Korea, under Grant 10077538.

ABSTRACT In this paper, a new comprehensive dynamic friction model for a collaborative industrial robot joint that considers the velocity, temperature, and load torque is proposed. The variation of load-dependent friction among the four-quadrant operation depending on the sign of load-torque and speed is studied. The new model's passivity property is analyzed to obtain a physically meaningful and experimentally identified friction model. A sufficient condition is presented in terms of a simple algebraic inequality involving the parameters of the model. The model parameter identification procedure and validation of model effectiveness are demonstrated experimentally on a commercial collaborative robot manipulator. Moreover, the proposed friction model's benefits are demonstrated in two different robot applications: friction compensation and direct teaching (smooth lead-through programming) applications. Significant tracking performance improvement in the root-mean-square errors up to 76% was achieved with the proposed friction model compared to the uncompensated cases in the friction compensation application. In the direct teaching application, the new model, which precisely estimates joint friction, results in a significant decrease in interaction forces up to 66%. These experimental results validate the performance of the proposed friction model.

INDEX TERMS Collaborative robot, friction model, human–robot interaction, manipulator dynamics, robot control.

I. INTRODUCTION

Actuation systems in collaborative robots rely on geared drive systems to obtain the relatively low-speed but high-torque mechanical output. Friction is one of the unavoidable side-effects of using a geared drive actuation system. Friction can severely deteriorate performance in terms of tracking errors, significant settling times, or limit cycles [1]–[5]. Therefore, friction compensation is indispensable to improve the performance of collaborative industrial robots. This is not only for tracking applications, but also for more advanced applications like estimation of contact forces for sensorless force control [6]–[8], sensitive collision detection [9], and force/torque sensorless direct teaching control [10]. Since the compensation technique is typically model-based, the knowledge of a suitable friction model that predicts the real friction is required. However, in general, friction model uncertainties and variations reduce the estimation reliability.

Friction is a complex phenomenon that arises when there is relative motion between two surfaces in contact. It can

The associate editor coordinating the review of this manuscript and approving it for publication was Yangmin Li.

be influenced by many factors such as geometry and permanency of contact between surfaces, the surfaces' material, and the lubricants used [11], [12]. To characterize the friction behavior, numerous static and dynamic friction models [13]–[17] have been studied and implemented, for example, in [18]. The LuGre model [16] is the most famous and widely used dynamic friction model. Nevertheless, the model does not include significant friction factors such as the effects of the actual contact surface and temperature variations.

Unlike industrial robots, a collaborative industrial robot shares its work-space with a human operator; therefore, a collaborative industrial robot must have special features such as collision detection and direct teaching. A fundamental issue is to build an accurate friction model of the robot joint to execute such tasks. The varying motions also directly affect the actuator temperature via the heat of the frictional losses, which has a significant variance. Although existing static or dynamic friction models have been effectively employed in industrial practice, there is a need to improve the collaborative robots' friction model due to the demands mentioned earlier.

The importance and inclusion of temperature, velocity, and load in static friction models have been addressed in [19]–[25].

However, these models do not cover the asymmetric load-dependent friction as a function of power flow. Consider a chain of power transmission in the axis of a robot (see Fig. 1). The direction of the power transmission defines the sign of P_A and P_B. $P_{Loss,i}$ is related to the friction torque τ_f defined in (3). In Fig. 1(a) since the power is transmitted from the motor to the mechanical axis, P_A is the input power, and P_B is the output power.

$$P_B = \frac{P_A}{1+\mu_1}, \qquad P_A > 0, \quad P_B > 0. \tag{1}$$

where the transmission system yield corresponds to $\mu = \mu_1$. On the other hand, Fig. 1(b) depicts the power transmission from the mechanical axis to the motor. For example, this is the case when the robot moves along the gravity direction. In this case, P_B is the input power, and P_A is the output power.

$$P_A = \frac{P_B}{1+\mu_2}, \qquad P_A < 0, \quad P_B < 0. \tag{2}$$

where the transmission system yield corresponds to $\mu = \mu_2$.

In general, $\mu_1 \neq \mu_2$, which implies that the transmission system yield depends on the sense of power transfer leading to two distinct sets of friction parameters. Therefore, the sliding friction torque is a linear function of both the dynamic and the external forces, with asymmetrical behavior depending on the signs of joint torque and velocity and a variation depending on the velocity amplitude (see Fig. 2). The measurement results in Fig. 2(a) depicts that the friction torque is less affected by the varying gravity load if speed and load torque do not have the same sign (areas shaded white). In contrast, a significant load-dependency of friction torque is manifested when the speed and the load torque have the same sign (areas shaded gray). In general, load-dependent friction is assumed to vary among the four-quadrant operation depending on the sign of load torque and speed.

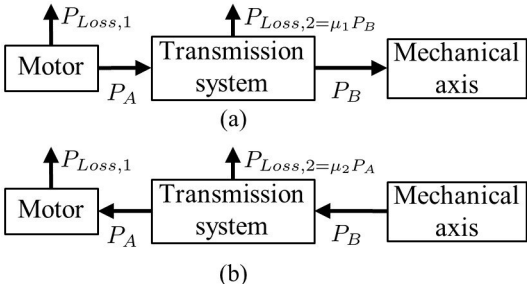

FIGURE 1. Power transmission in a chain.

Most importantly, the passivity property of such a comprehensive model has not been reported. Load- and temperature-dependent friction modeling is typically based on experimental observation. This process involves choosing a function that fits the experimental data and estimating the parameters of the model. Indeed, a model is expected to describe a physical process; hence, the approach of a simple curve fitting method is incongruous. Therefore, the model must satisfy a fundamental property of defining input-output passive operator, reflecting power dissipation's physical property.

Because of the issues mentioned above and the demand for improving the task related to a collaborative industrial robot, developing a more realistic friction model is required. In this work, a comprehensive friction model for a collaborative industrial robot joint is developed. The details of the introduction of load and temperature effects in friction representation models for the robot joint are presented. The proposed model includes the direction dependency of friction coefficients and an advanced load dependency model motivated by the measurement results shown in Fig. 2.

Furthermore, the proposed model's passivity property is analyzed, and a sufficient condition is found in terms of algebraic inequality involving the model's parameter. The constraint is imposed in the identification algorithm, resulting in a physically meaningful friction model. The benefit of an improved friction model was shown in both tracking and direct teaching applications. As experimental results verify, the new model allows quantifying friction effects in the robot joint with a high accuracy level.

The remainder of the paper is organized as follows. Section II presents a problem description. In Section III, the proposed friction model is detailed, whereas Section IV presents the passivity analysis of the friction model. Experimental results and conclusions are presented in Sections V and VI, respectively.

II. PROBLEM DESCRIPTION

Consider a manipulator that can be described by the standard dynamic equation

$$\mathbf{M}(\mathbf{q})\ddot{\mathbf{q}} + \mathbf{C}(\mathbf{q}, \dot{\mathbf{q}})\dot{\mathbf{q}} + \mathbf{G}(\mathbf{q}) + \boldsymbol{\tau}_f = \boldsymbol{\tau}_m, \tag{3}$$

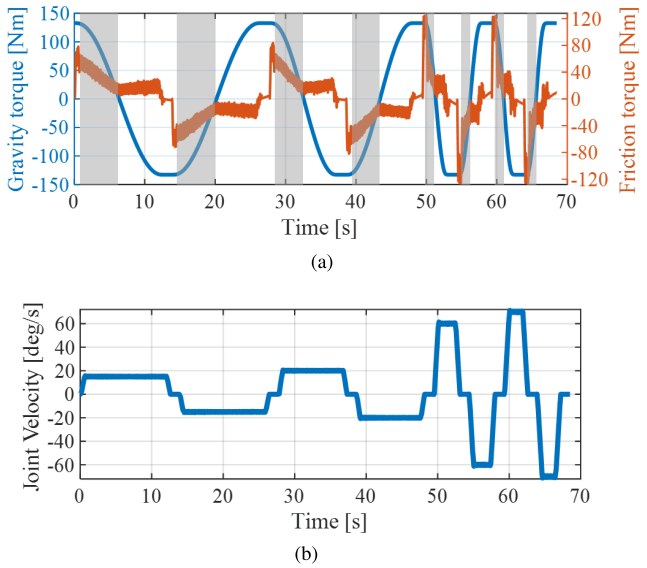

FIGURE 2. Load dependence of friction. (a) Recorded friction (dusty orange) during the back-and-forth motion of a joint at different constant speeds with considerable gravity load variation (dusty blue). Load dependency has a different pattern for motoric duty (shaded gray) and generatoric duty (shaded white). Furthermore, load dependency varies with speed. (b) Velocity trajectory used for identification of load-dependent friction.

where $\boldsymbol{q} \in \mathbb{R}^{N_{DOF}}$ represents the N_{DOF} joint angles, $\mathbf{M}(\mathbf{q})$ is the inertia matrix, $\mathbf{C}(\mathbf{q}, \dot{\mathbf{q}})$ captures the centrifugal and Coriolis effects, $\mathbf{G}(\mathbf{q})$ represents the gravitational torque, and $\boldsymbol{\tau}_f$ is a friction torque which includes all torque related to dissipated power at the joint. The drive torque $\boldsymbol{\tau}_m$ applied by the joint motor controls the system. The drive torque is obtained by multiplying the motor current measurements by the torque constant of the motor. Once the motor torque $\boldsymbol{\tau}_m$, the inertia term $\mathbf{M}(\mathbf{q})$, and the Coriolis term $\mathbf{C}(\mathbf{q}, \dot{\mathbf{q}})$ are known, friction torque $\boldsymbol{\tau}_f$ can be obtained from (3). Moving one joint at a time at a constant speed makes the coupling effects included in the Coriolis and the inertia terms negligible. Now, the simplified form of (3) becomes

$$\boldsymbol{\tau}_f = \boldsymbol{\tau}_m - \boldsymbol{G}. \tag{4}$$

Throughout the paper, it is assumed that the DH- and gravity parameters (i.e., the center of gravity and mass of each link) and therefore $\boldsymbol{G}$ are known accurately.

A. EXTENSION OF DYNAMIC FRICTION MODELS

It is argued in [26] that dynamic models are necessary to describe the friction phenomena better. The friction phenomenon by nature exhibits a nonlinear continuous behavior during velocity zero-crossing, unlike the static friction models that are discontinuous at velocity reversal. Therefore, it is better to use a dynamic friction model that encompassed dynamic phenomena for a smooth transition and a better description of friction phenomenon. Following this demand, we extended the generic form of a dynamic friction model $\boldsymbol{\tau}_f$ that takes into account internal state z (possibly multi-states), velocity-, load-, quadrant-, and temperature-dependent effects, *i.e.*. for each joint

$$\tau_{f,i} = \delta(z_i) + \zeta(\dot{q}_i, T_i, \tau_{L,i}), \qquad i = 1, \cdots, N_{DOF}. \tag{5}$$

Therein, $\delta(z_i)$ is a function responsible for the transient velocity response, $\zeta(\dot{q}_i, T_i, \tau_{L,i})$ is the load-, quadrant-, and temperature-dependent velocity strengthening function, T_i represents the joint temperature, and $\tau_{L,i}$ is the external joint load comprising gravity and dynamic load. From now on, we use a plain symbol without subscript i as all consideration is for a single joint unless stated otherwise.

The state equation that describes the dynamics of the internal state vector z is a first-order differential equation of the form

$$\frac{dz}{dt} = h(z, \dot{q}). \tag{6}$$

This state captures the transient response with respect to the velocity. For constant velocities, the function $h(z, \dot{q}) = 0$ and equation (5) will converge to a static friction torque

$$\tau_{f,s} = g(\dot{q})sgn(\dot{q}) + \zeta(\dot{q}, T, \tau_L). \tag{7}$$

where $g(\dot{q})$ is a velocity weakening function (Stribeck effect). $sgn(\dot{q})$ is the signum function defined as follows:

$$sgn(\dot{q}) = \begin{cases} -1, & \text{if } \dot{q} < 0 \\ 0, & \text{if } \dot{q} = 0 \\ 1, & \text{if } \dot{q} > 0 \end{cases}$$

The generic form of the function $g(\dot{q})$ is given by

$$g(\dot{q}) = (F_c + (F_s - F_c)e^{-\frac{\dot{q}^2}{v_s^2}}). \tag{8}$$

where F_c is Coulomb friction, F_s is stiction, and v_s is Stribeck velocity.

LuGre model is a special case of generic form dynamic friction model (5) where the velocity strengthening function (viscous friction) is expressed as a linear proportional to the relative velocity. In this model, since the friction between two surfaces is considered as a contact between bristles, the variable z denotes these bristles' average deflection. As a result of this, the function $\delta(z)$ represents the friction force generated by the bristles bending. The expression of this function is given by

$$\delta(z) = \sigma_0 z + \sigma_1 \dot{z} \tag{9}$$

where, σ_0 is the bristle stiffness and σ_1 is the micro-damping coefficient. The state equation that describes the dynamics of the internal state z is given by

$$\frac{dz}{dt} = \dot{q} - \sigma_0 \frac{|\dot{q}|}{g(\dot{q})} z. \tag{10}$$

This paper aims to develop the extended-term $\zeta(\dot{q}, T, \tau_L)$ so that the comprehensive friction model describes the robot joint friction phenomena accurately. In fact, the new model is expected to satisfy a fundamental property of defining input-output passive operators. For an input-output model

that describes a physical process and that gets all its energy from the input, to be generally accepted, it ought to be passive since that is how nature works. Intuitively it may be expected that friction is passive (dissipates energy). The energy consumed by the friction is given by

$$\int \tau_f dq = \int \tau_f \dot{q} dt$$

Since the friction model given by (5) is dynamic, there may be aspects where friction stores energy and others where it gives energy back. It is, therefore, interesting to see if it is possible to find a nonnegative function $V(z(t))$ such that

$$\int_0^t \tau_f \dot{q} dt \geq V(z(t)) - V(z(0)).$$

This implies that the friction τ_f is passive (friction dissipates energy) [27], [28]. We will now take a closer look at some passivity properties of the friction model in (5).

Property 1: For a passive operator $\sum : L_2 \longrightarrow L_2 : \dot{q} \longrightarrow \tau_f$ *defined by dynamic system (5), (8), (9), and (10) with respect to the function* $V(z(t)) = \sigma_0 z^2(t)/2$ *we have*

$$\Phi(0,t) = \int_0^t \tau_f \dot{q} dt \geq V(z(t)) - V(z(0)) \tag{11}$$

for all $\dot{q} \in L_2$ *and all* $t \geq 0$*, if*

1) *the damping coefficients are restricted to* $0 \leq \sigma_1 \leq 4g(\dot{q})/|\dot{q}|$*, and*
2) *the product of* $\zeta(\dot{q}, T, \tau_L)$ *and* $\dot{q}$ *is nonnegative.*

Proof: See Section IV. ■

Here, if the passivity property of the friction model is satisfied, the function $V(z(t)) = \sigma_0 z^2(t)/2$ can be used as one candidate Lyapunov function to analyze the stability of the overall closed-loop system with friction compensation. In general, this paper aims to develop a newly introduced parametric model $\zeta(\dot{q}, T, \tau_L)$ that takes into account velocity-, load-, quadrant-, and temperature-dependent effects subject to the passivity requirement.

III. PROPOSED FRICTION MODELING

This section presents thorough discussions on the modeling of the newly introduced function $\zeta(\dot{q}, T, \tau_L)$ that captures the nonlinear viscous and load-, quadrant-, and temperature-dependent effects from both theoretical and experimental perspective.

A. NONLINEAR VISCOUS FRICTION MODEL

Depending on the system behavior, different expressions that describe the viscous part of the static friction model exist, e.g. [13], [29]. The most typical friction contacts in robotic actuation are the lubricated friction contacts in the main harmonic drive (HD). The friction in HD was investigated in [30] and found to have a strongly nonlinear viscous friction dependency. In fact, joint temperature variation results in a significant change in the viscous friction for the same joint speed. Therefore, the parameters of a given nonlinear viscous friction model should be a function of joint temperature. Consequently, in addition to fitting experimental data, the choice of the expression for viscous friction requires considering the model sensitivity for a small deviation on the model parameters.

During experiments, we observed that the torque-velocity map is not symmetric for negative and positive velocity. Generally, such asymmetry happens because the asperity at the contact point for a moving object might not be the same during forward and reverse motion.

Afterward, an exponential model is proposed to map the nonlinear viscous behavior over the velocity range (12).

$$f_v(\dot{q}) = \begin{cases} \sigma_{2,p}(1 - e^{-|\frac{\dot{q}}{\sigma_{3,p}}|}) & \dot{q} > 0 \\ \sigma_{2,n}(1 - e^{-|\frac{\dot{q}}{\sigma_{3,n}}|}) & \dot{q} < 0 \end{cases} \tag{12}$$

This model depends on the speed and direction of rotation (differing coefficients for positive, p and negative, n directions are used, i.e., $\sigma_{2,p}$, $\sigma_{2,n}$, $\sigma_{3,p}$ and $\sigma_{3,n}$).

B. TEMPERATURE AND LOAD DEPENDENT FRICTION MODEL

1) TEMPERATURE-DEPENDENT FRICTION MODEL

Friction in HD tends to decrease significantly at high temperatures. This observation is assumed to be caused by a change in the contact point properties and the lubrication layer thickness. At low temperatures, the expansion of solids affects the amount of preloading. This consequently affects the behavior of viscous friction. Besides, a good illustration of the effect of temperature can be observed from HD manufacturers' efficiency data.

Since the temperature variation mainly influences viscous friction, the proposed nonlinear viscous model parameters become a function of joint temperature. Thus, an expression for viscous friction as a function of joint velocity and joint temperature, which is called the velocity-temperature model, is proposed as follows:

$$f_v(\dot{q}, T) = \begin{cases} f_{v,p}(\dot{q}, T) = \sigma_{2,p}(T)(1 - e^{-|\frac{\dot{q}}{\sigma_{3,p}(T)}|}) & \dot{q} > 0 \\ f_{v,n}(\dot{q}, T) = \sigma_{2,n}(T)(1 - e^{-|\frac{\dot{q}}{\sigma_{3,n}(T)}|}) & \dot{q} < 0 \end{cases} \tag{13}$$

where $\sigma_{j,p}(T) = \sigma_{jo,p} + \sigma_{jT,p}T$, and $\sigma_{j,n}(T) = \sigma_{jo,n} + \sigma_{jT,n}T$, for $j = 2, 3.$, is a temperature-dependent viscous friction model parameters, and T is the temperature (°C) of the joint.

2) LOAD-DEPENDENT FRICTION MODEL

In a robot actuation transmission mechanism, the torque is transmitted through the contacts between solids. The true contact surface varies according to the applied normal forces between the two surfaces in contact. This causes the friction related to the interaction between the contacting surfaces to vary according to the applied normal force. For joint torques in a robot with a revolute joint, only the load torque aligned with the joint rotation axis affects the joint friction. This load on the robot axis comprises a holding torque caused by gravitational force, dependent on the robot's kinematic

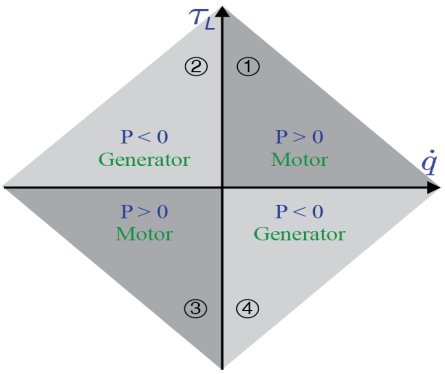

FIGURE 3. Power quadrant operation.

position, and a load torque caused by external forces applied to the robot.

Friction depends linearly on the absolute value of the load [31]. In fact, for the same load, joint speed variation results in different joint friction. Considering such experimental observations and the fact that friction has a linear relation with the absolute value of the load, the following first-order polynomial expression is proposed.

$$\eta(\dot{q}, \tau_L) = (\beta(\dot{q}) + \alpha(\dot{q})|\tau_L|)\text{sgn}(\dot{q}) \tag{14a}$$

where $\beta(\dot{q})$ and $\alpha(\dot{q})$ are the two function to be identified, and τ_L is the external joint load comprising gravity and dynamic load. With $|\tau_L| = \tau_L \text{sgn}(\tau_L)$ and $\text{sgn}(\tau_L)\text{sgn}(\dot{q}) = \text{sgn}(\tau_L\dot{q})$, (14a) becomes:

$$\eta(\dot{q}, \tau_L) = (\beta(\dot{q}) + \alpha(\dot{q})\tau_L)\text{sgn}(\tau_L\dot{q}) \tag{14b}$$

Load-dependent friction is sensitive to the quadrant operation, whether power flows from the power source to the load (opposite load) or from the load to the power source (aiding load). The expression in (14b) is called the power sign-dependent friction model. Depending on the sign of the output power denoted by $P = \tau_L\dot{q}$, one can define four quadrants that can be categorized into two-quadrant operation groups called motor and generator (Fig. 3). In quadrants 1 and 3, P is positive, and the actuator exhibits a motor behavior. In quadrants 2 and 4, P is negative, and the actuator exhibits a generator behavior. Consequently, a model structure in (15) is proposed for load-dependent friction.

$$\eta(\dot{q}, \tau_L) = \begin{cases} \beta_1(\dot{q}) + \alpha_1(\dot{q})\tau_L & \dot{q} > 0, \tau_L > 0 \\ \beta_2(\dot{q}) + \alpha_2(\dot{q})\tau_L & \dot{q} < 0, \tau_L > 0 \\ \beta_3(\dot{q}) + \alpha_3(\dot{q})\tau_L & \dot{q} < 0, \tau_L < 0 \\ \beta_4(\dot{q}) + \alpha_4(\dot{q})\tau_L & \dot{q} > 0, \tau_L < 0 \end{cases} \tag{15}$$

where

$$\beta_i(\dot{q}) = \gamma_{1,i}(1 - e^{-|\gamma_{2,i}\dot{q}|}) + \gamma_{3,i}$$
$$\alpha_i(\dot{q}) = \lambda_{1,i} + \lambda_{2,i}\dot{q} \qquad \text{for } i = 1, 2, 3, 4.$$

are load-dependent friction model parameters.

Since these parameters are velocity dependent, Equation (15) is called the velocity-load model.

C. COMPREHENSIVE FRICTION MODEL

A comprehensive friction model is derived after a careful investigation of the nonlinear viscous, load, quadrant-operation, and temperature dependencies are made. The experimental results at constant low speeds indicate that the stiction is small or even negligible in the system with HD [32], [33]. Consequently, the expression for velocity weakening function is simplified to

$$g(\dot{q}) = F_c m(\dot{q}), \qquad F_c = \begin{cases} F_{c,p} & \dot{q} > 0 \\ F_{c,n} & \dot{q} < 0 \end{cases} \tag{16}$$

Therein, $m(\dot{q}) = \frac{2}{\pi} arctan(k\dot{q})$ with k being a positive constant.

Remark 1: In the real environment, a static friction torque needs to be taken into consideration. However, the friction torque of a robot joint module is generated mostly in a harmonic drive. Since such a transmission system is usually sufficiently lubricated, the stiction is negligible. In this case (8) is simplified to (16). Nevertheless, when there is significant stiction in the system we can use (8) to express velocity weakening function $g(\dot{q})$.

Combining (13) and (15), the expression of a function $\zeta(\dot{q}, T, \tau_L)$ is given by:

$$\zeta(\dot{q}, T, \tau_L) = f_v(\dot{q}, T) + \eta(\dot{q}, \tau_L) \tag{17}$$

Consequently, a comprehensive friction model structure becomes:

$$\tau_f(\dot{q}, T, \tau_L) = \sigma_0 z + \sigma_1 \dot{z} + f_v(\dot{q}, T) + \eta(\dot{q}, \tau_L) \tag{18}$$

Remark 2: The $z(t)$ evolution may be obtained by either integrating the nonlinear differential equation numerically (10) or applying a proper discretization. The former procedure is presently adopted.

IV. PASSIVITY ANALYSIS OF FRICTION MODEL

In this section, the passivity property of a nonlinear friction model is studied. The passivity property of friction is essential to stabilize the closed-loop control system during the design of the friction compensator. The major advantage of defining the passivity property for a friction model is that it enables a control law to be developed separately from the friction compensator design, provided that each part satisfies some passivity properties. In other words, a feedback/feed-forward friction compensation to a passive closed-loop system preserves passivity, which results in an asymptotically stable closed-loop system together with a feedback friction compensation [15], [34].

Considering the proposed friction model (18), proof for Property 1 is presented as follows.

Proof: Now, we will evaluate (11) splitting it into two terms $\Phi = \Phi_1 + \Phi_2$ with

$$\Phi_1(0, t) \equiv \int_0^t (\sigma_0 z + \sigma_1 \dot{z})\dot{q} dt$$

and

$$\Phi_2(0,t) \equiv \int_0^t \zeta(\dot{q}, T, \tau_L)\dot{q}dt$$

Rearranging and replacing $\dot{q}$ from (10) in Φ_1 we get

$$\begin{aligned}
\Phi_1(0,t) &= \int_0^t (\sigma_0 z + \sigma_1 \dot{z})(\dot{z} + \sigma_0 \frac{|\dot{q}|}{g(\dot{q})} z)dt \\
&= \int_0^t (\sigma_0 z\dot{z} + \sigma_1(\dot{z}^2 + \sigma_0 \frac{|\dot{q}|}{g(\dot{q})} z\dot{z}) + \sigma_0^2 \frac{|\dot{q}|}{g(\dot{q})} z^2)dt \\
&= \int_0^t (\sigma_0 z\dot{z} + \sigma_1(\dot{z} + \sigma_0 \frac{|\dot{q}|}{2g(\dot{q})} z)^2 \\
&\quad + \sigma_0^2 \frac{|\dot{q}|}{g(\dot{q})} z^2 - \sigma_1(\sigma_0 \frac{|\dot{q}|}{2g(\dot{q})} z)^2)dt \\
&\geq \int_0^t (\sigma_0 z\dot{z} + \sigma_0^2 \frac{|\dot{q}|}{g(\dot{q})}(1 - \sigma_1 \frac{|\dot{q}|}{4g(\dot{q})})z^2)dt \\
&\geq \frac{1}{2}\sigma_0 z^2(t) - \frac{1}{2}\sigma_0 z^2(0)
\end{aligned}$$

if the damping coefficient $\sigma_1 \leq 4g(\dot{q})/|\dot{q}|$.

For the other term, we replace $\zeta(\dot{q}, T, \tau_L)$ from (17) and use (13) and (15)

$$\begin{aligned}
\Phi_2(0,t) &= \int_0^t (f_v(\dot{q}, T) + \eta(\dot{q}, \tau_L))\dot{q}dt \\
&= \int_0^t (f_v(\dot{q}, T)\dot{q} + \eta(\dot{q}, \tau_L)\dot{q})dt \\
&\geq 0
\end{aligned}$$

if

- the viscous coefficients are restricted to $\sigma_{2,p}(T) > 0$ and $\sigma_{2,n}(T) < 0$, and
- the load-dependent friction parameters are restricted to $\alpha_1(\dot{q}), \alpha_3(\dot{q}) > 0$, and $\alpha_2(\dot{q}), \alpha_4(\dot{q}) > 0$.

■

It is evident that when velocity increases from the first condition, at some velocity value damping coefficient becomes larger. If we use a fixed damping coefficient, this condition does not hold anymore. If the damping coefficient σ_1 decreases for increasing velocity,e.g.,

$$\sigma_1(\dot{q}) = \sigma_1 e^{-|\frac{\dot{q}}{v_d}|}$$

a passive model can be obtained, which is physically motivated by the change of the damping characteristics as velocity increases. $v_d = 0.001$, which determines the velocity interval around zero where there is damping, is chosen in order to have high damping for zero velocity (see [35]).

V. EXPERIMENTAL RESULTS

In this study, experiments were conducted using a commercial 6-DOF collaborative robot manipulator (called Indy7 [36]). Robot joints are actuated using six brush-less DC motors with HD. A 16-bit multiturn absolute encoder measures each angular position. An electric current detection module designed based on the shunt current sensing method is used to measure motor current. The joint torque is determined by multiplying the measured motor current by the torque constant of the motor. The robot has an integrated joint containing a direct drive frameless motor, strain wave gear set, a high-resolution encoder, brake, and integrated motor control electronics, including a temperature sensor as a single joint module. This temperature sensor is used for temperature-dependent friction modeling. The reference trajectories and data acquisition of each joint were updated at a sampling frequency of 4 kHz.

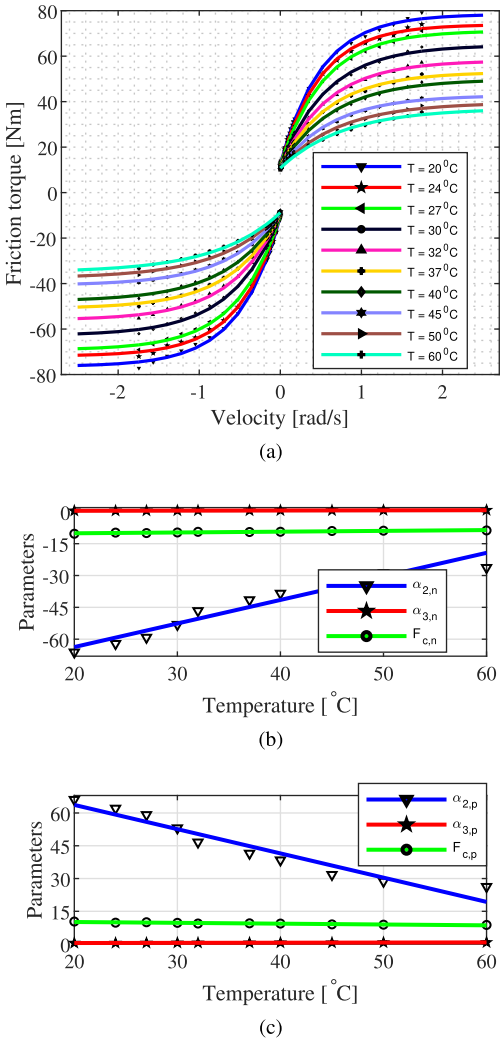

FIGURE 4. The dependency of friction on velocity and temperature for joint 2. (a) static friction: experimental data (markers) and *model fit* (solid lines) corresponding to (20) for different individual joint temperature values. (b) and (c) depicts the variation of model parameters as a function of joint temperature for negative and positive velocity, respectively. The model parameters change with respect to the joint temperature are indicated with markers, and *model fit* corresponding to the equation of parameters described in (13) are indicated with solid lines.

A. FRICTION PARAMETER IDENTIFICATION

1) FIRST IDENTIFICATION STEP

During the identification of model parameters, an intensive experimental study was performed to obtain insights and separate dependencies in the velocity, temperature, and load. First, the joint under investigation is rotated back and forth

at different constant speeds. However, the other joints of the manipulator are placed in a configuration that results in the joint under investigation remained not subjected to gravitational load, i.e., a joint whose motion axis is perpendicular to the ground. Subsequently, (4) can be simplified, and the friction torque for a single joint can be obtained as

$$\tau_m = \tau_f \tag{19}$$

i.e., the measured torque is equal to the friction torque.

The velocity-temperature model (13) parameters are identified under this experimental procedure. Experimental data is collected by manipulating different constant velocity points covering the considered velocity range over different constant temperatures and observing the average of the resultant torques. The temperature deviation during every individual experiment is maintained at ≤ 1 °C, which is assumed as an acceptable uncertainty. The Levenberg-Marquardt algorithm in the optimization toolbox of MATLAB is employed in the identification process of velocity-temperature model parameters.

The collected data is used to identify different temperature-independent friction curves (20)

$$f_v(\dot{q}) + g(\dot{q}) = \begin{cases} F_{c,p} + \sigma_{2,p}(1 - e^{-|\frac{\dot{q}}{\sigma_{3,p}}|}) & \dot{q} > 0 \\ F_{c,n} + \sigma_{2,n}(1 - e^{-|\frac{\dot{q}}{\sigma_{3,n}}|}) & \dot{q} < 0 \end{cases} \tag{20}$$

to gain insights into the parameter changes for the joint temperature variation (see Fig. 4(b,c)). The markers indicate the parameters of the temperature-independent models that have been identified at single temperature values. A linear equation was discovered to sufficiently represent the parameter variation in the temperature (depicted with solid lines). Since all the other joints of the robot exhibit similar trends, only the result for joint 2 is presented in Fig. 4. The temperature range during this identification experiment was limited from 20°C to 60°C because of the limitations of the experimental environment. From the experimental results, we observed that the variation in the Coulomb friction with the temperature change is negligible. This shows that the significant influence of temperature variation is on viscous friction, which supports the proposed velocity-temperature model (13).

The overall output of the proposed velocity-temperature model (13) is illustrated in Fig. 4(a).

2) SECOND IDENTIFICATION STEP

In the second experiment, the joint under investigation is rotated back and forth between the limiting position range $\pm$ 90° at different constant speeds. The motion is designed to maximize the variation of gravity load on the joint of interest, see Fig. 5. From (4), the friction torque for a single joint can be indirectly obtained as

$$\tau_f = \tau_m - \tau_g \tag{21}$$

where τ_g is joint gravity torque.

The load-dependent friction is obtained by subtracting the friction in (20) from the total friction expressed in (21).

FIGURE 5. Indy-7 collaborative industrial robot: Measurement scheme to identify the load-dependent friction parameters for joint 2, and experimental conditions used to verify the teaching method.

TABLE 1. Quality evaluation for different friction models.

	Standard model (22)	Comprehensive model (18)
$e_{d,\text{RMS}}$	1.1276	0.3507

Twenty-two different data points are collected at different constant velocity points encompassing the considered velocity range with full payload variation. The friction change with a load variation is shown in Fig. 1. It is noticeable that the friction torque is affected less by varying gravity load if speed and load toque do not have the same sign (areas shaded white), while a significant load-dependency of friction torque is visible if speed and load torque have the same sign (areas shaded gray). In addition to that, Fig. 1 shows that load dependency can also vary with speed.

The measured data are grouped into four quadrants based on the sign of the gravity load and the motion direction. A first-order polynomial is found to be sufficient to represent the load-dependent friction change with load variation at each quadrant. Load-dependent parameters β_i and α_i for $i = 1, 2, 3,$ and 4, which represent the four quadrants, is identified at each constant velocity. This facilitated identifying the behavior of the individual parameters for the velocity change shown in Fig. 6(a,b). The Levenberg-Marquardt algorithm in the optimization toolbox of MATLAB is employed to identify the velocity-load model parameters. To evaluate the quality of the friction model, the proposed comprehensive friction model (18) is compared with the standard LuGre model. Neglecting the effect of the load and the temperature, friction model (5) can be reduced to a standard LuGre model

$$\tau_f = \sigma_0 z + \sigma_1 \dot{z} + \sigma_4 \dot{q} \tag{22}$$

where σ_4 is viscous coefficient. Both models are parameterized to fit the same identification data. Fig. 7 depicts the model fit and model error for the two different models. The proposed comprehensive friction model outperforms the standard model because a significant load dependency is evident. Furthermore, to quantify the model quality, the RMS of the model error, $e_{d,\text{RMS}}$, is computed and compared between the two models, as shown in Table 1. Table 1 indicates that the model quality is improved significantly up to 69% by considering the load effect during friction modeling.

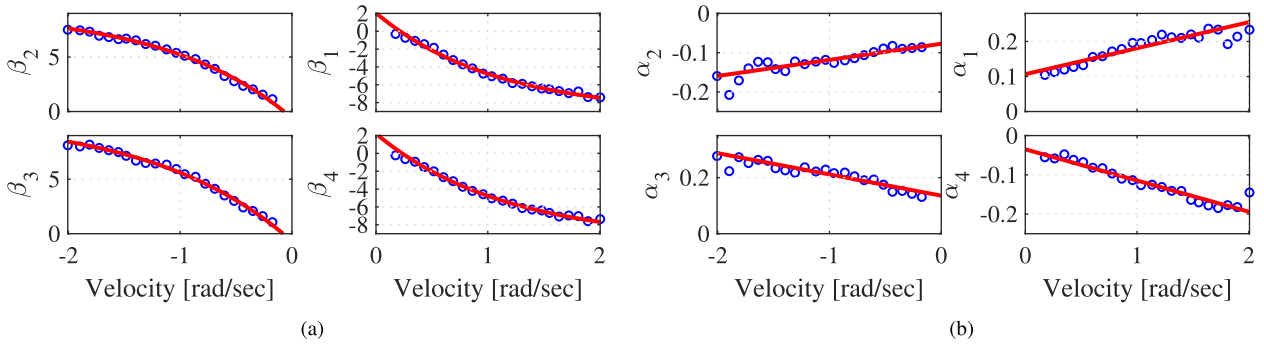

FIGURE 6. Load-dependent parameters at different constant velocity points for each quadrant operation of joint 2. The parameter change (with blue markers) is modeled (with red solid line) to map the velocity dependency as in equation (15) (a,b).

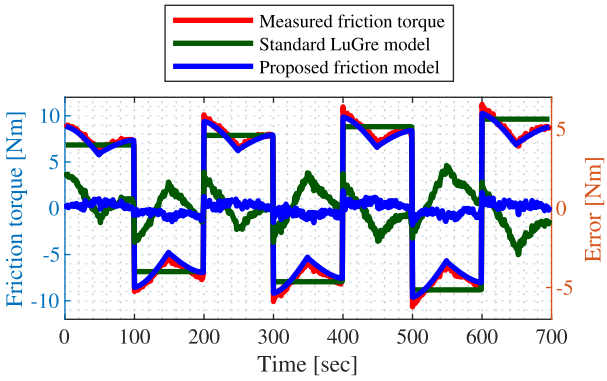

FIGURE 7. Model quality comparison of Joint 2. Measured friction torque (red) is compared with those of different friction models. The standard model (22) does not capture the significant load dependency (dark green). The plot against the right y-axis shows that the model error for the load-dependent model (blue) is significantly reduced compared to the standard model error (dark green). The load-dependent model (18) captures load dependency with a better model accuracy (blue).

3) DYNAMIC MODEL IDENTIFICATION

The dynamic behavior of the proposed friction model is thoroughly characterized, using σ_0 and σ_1, which correspond to the fictitious bristle stiffness and damping, respectively. An open-loop experiment is performed with a sinusoidal torque input (the input torque is smaller than the Coulomb friction torque and varies slowly). A more detailed information can be found in [37]. The Nelder-Mead generalized pattern search algorithm in MATLAB optimization toolbox has been used to determine the dynamic parameters, σ_0 and σ_1, of the proposed comprehensive friction model (18).

Table 2 reports the estimated values of the dynamic friction parameters for the six joints of the Indy-7 robot.

TABLE 2. Estimated parameters of the dynamic friction model.

	Joint-1	Joint-2	Joint-3	Joint-4	Joint-5	Joint-6
σ_0	16804	12930	1820	1649	1106	985
σ_1	270	233	105	81	72	68

B. APPLICATIONS BASED ON THE FRICTION MODEL

1) FRICTION COMPENSATION

The proposed friction model's effectiveness is demonstrated by applying a feedback model based on friction compensation, which benefits from accurate friction estimations (see Fig. 8). The desired joint trajectory is generated, as shown in Fig. 9. To prove the necessities of considering load and temperature effects on friction, experiments are carried out at high joint temperature (a minimum of 45 °C for joint 1 and a maximum of 55°C for joint 5), with an additional payload of 6.66 kg added to the robot.

The control scheme described in [38], originally proposed to achieve high motion control performances and robustness even in the presence of disturbances and model uncertainties, is used in this study for friction compensation. A model-based H_∞ PID controller is applied as follows:

$$\tau_m = \hat{M}(q)\ddot{q}_r + \hat{C}(q,\dot{q})\dot{q}_r + \hat{g}(q) + \tau_{ref}, \tag{23}$$

where $\hat{M}, \hat{C}$ and $\hat{g}$ denote the nominal model parameters, $\dot{q}_r = \dot{q} + K_p e + K_I \int e dt$ represents the reference trajectory, $e = q_d - q$ is the position error, q_d represents the desired trajectory, and τ_{ref} is the optimal control input given as

$$\tau_{ref} = -(K + \frac{1}{\gamma^2})\dot{e}_r \tag{24}$$

$$= -(K + \frac{1}{\gamma^2})(\dot{e} + K_p e + K_I \int e dt) \tag{25}$$

where $\gamma > 0$ and $K, K_I, K_p > 0$ are diagonal gain matrices satisfying $K_p^2 > 2K_I$ (for details, see [38]).

During the experiment, the actual joint position is measured, and the controller's tracking performance with different friction models is compared. The experiment is performed for three cases; first without friction compensation, then with friction compensation according to (22), and finally with friction compensation according to (18). The same control parameters, which are optimally tuned, were used during all three cases. All experimental procedures are performed in the current control mode. Fig. 10 shows error distribution comparison for the three cases. The tracking error distribution shows the maximum, median (black line inside of each box), minimum, and the box, representing where the 50% of the error falls. Experimental results show that neglecting the temperature and load dependency during friction modeling results in a root-mean-square error of up to 70% from the commanded position. Thanks to the improved friction model, joint position tracking performance increased up to 76% on

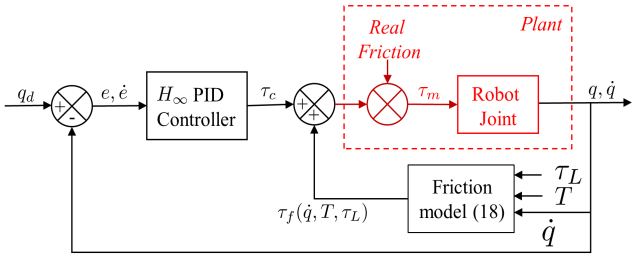

FIGURE 8. Trajectory tracking control scheme with H_∞ PID controller and a model-based feedback friction compensator. The "real friction" block illustrates the effect of real friction on the joint actuator. "Plant" is the robot joint actuator. A feedback compensator estimates the friction based on the joint velocity, $\dot{q}$, joint temperate, T, and joint gravity torque, τ_L, depending on the current robot configuration, and cancels out the effect of friction.

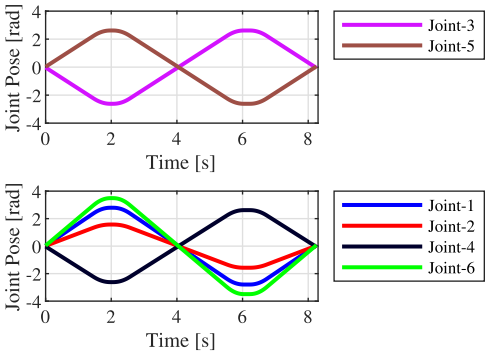

FIGURE 9. Joint space desired trajectory for friction compensation experiment.

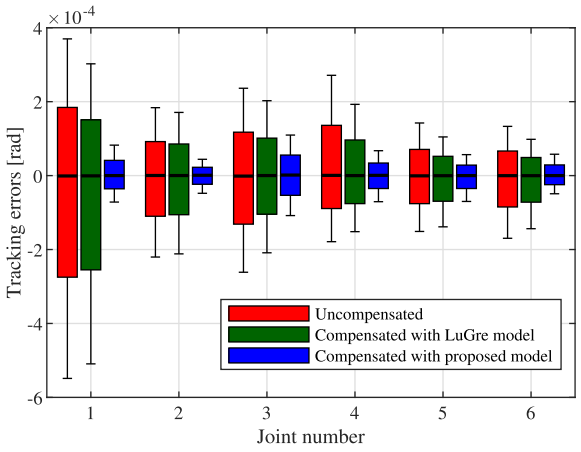

FIGURE 10. Friction compensation performance comparison. Tracking error distribution for each joint with maximum, median (black line inside of each box), minimum, and interquartile range.

the root-mean-square errors comparing to the uncompensated control.

2) DIRECT TEACHING WITH FRICTION AND GRAVITY COMPENSATION

Most collaborative robots can be programmed by the teach-and-playback method, in which the user can literally take the robot by hand and guide it to the desired goal point of its tool center point. The most simple direct teaching scheme can be achieved by compensating the gravity- and friction-induced torques. To improve responsiveness, friction can partially be compensated by

$$\tau_m = \tau_g + \alpha_{fric}\tau_f, \quad 0 \le \alpha_{fric} \le 1, \tag{26}$$

where α_{fric} is a friction compensation factor.

A direct teaching scheme in (26) is a completely open loop, and thus if the estimated desired torque is larger than the required torque, the manipulator can accelerate and become unstable. Therefore, the friction factor α_{fric} has to be tuned to a reasonable value in order not to overcompensate friction in the general case. Since friction changes substantially over a long robot operation due to a temperature rise, typically, α_{fric} tuned to a relatively small value, such as $\alpha_{fric} \approx 0.35$. Thanks to the improved friction model (18), the compensation factor can be increased up to $\alpha_{fric} \approx 0.85$ without any overcompensation. This allows us to decrease interaction forces substantially and almost have the manipulator free-floating.

Experiments are carried out to investigate the magnitude of the interaction force required to guide the manipulator to a desired joint position. A force/torque sensor installed at the end of the manipulator is used to measure the magnitude of external force applied by the operator to guide the manipulator to the desired point (see Fig. 5). The experiment is performed two times; first with friction compensation according to (22), and finally with friction compensation according to (18). During this experiment, the joint temperature was at 27°C; hence, a more substantial external force is required as a result of an increase in friction due to low joint temperature. Taking the friction compensation in high joint temperature case into account, α_{fric} is tuned and set to 0.35 when a LuGre friction model (22) used. Likewise, α_{fric} is tuned for the new friction model (18). Since model (18) allows quantifying friction effects in the joint with a high level of accuracy, the value of α_{fric} was increased to 0.85 without any overcompensation.

Without loss of generality, only joint 2, which covers considerable load variation, is manually moved while the other joints are locked, see Fig 5. The manipulator is guided (the handle attached to the force/torque sensor as shown in Fig. 5 is used) at velocity about 34 deg/s for all cases. The interaction force needed to manually move joint 2 of the manipulator from -90° to 90° is compared to show how the new model precisely estimates friction and significantly decreases interaction force, see Fig. 11. Using the standard friction model (22) resulted in a larger interaction force up to 48 N, see Fig. 11(a). For the same experiment, except where the joint velocity was approximately kept about 34 deg/s in both cases, the proposed friction model(18) allowed to reduce interaction force up to 66%, which enable the operator to guide the robot fast with less effort, see Fig. 11(b).

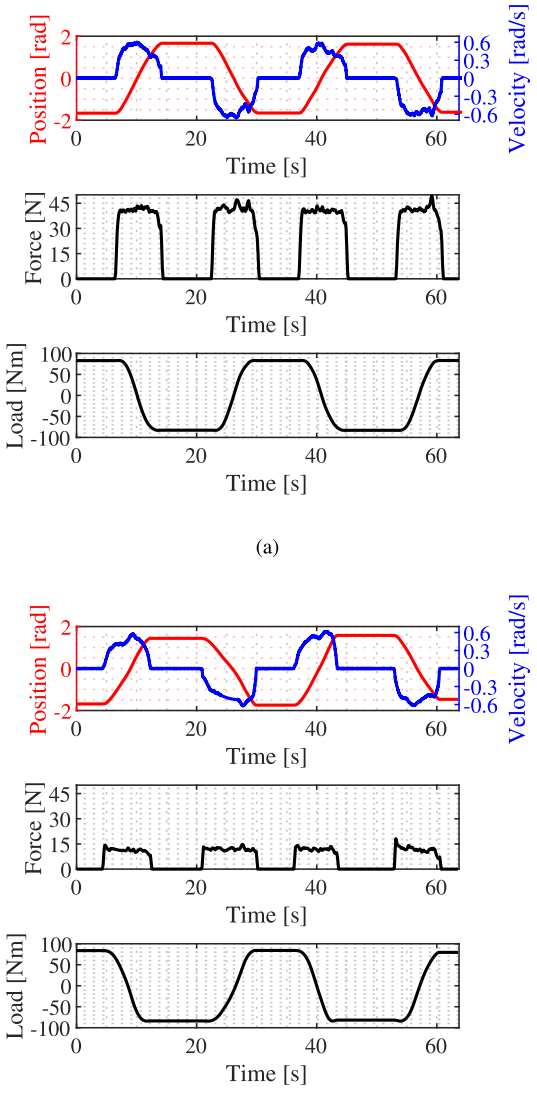

FIGURE 11. External force guiding joint 2 from position −90° to 90° at 27°C joint temperature. (a) With friction compensation according to (22); joint position (red) and velocity (blue), magnitude of interaction force (middle) and load variation. (b) With friction compensation according to (18); joint position (red) and velocity (blue), magnitude of interaction force (middle) and load variation.

VI. CONCLUSION

A modified empirically motivated friction model for a robotic joint has been presented. A velocity-dependent generalized empirical friction model is introduced to capture the non-linear thermal dependency, external load dependency, and quadrant of operation dependency of the friction model. An extensive experimental study has been conducted to identify the parameters of the model to capture all friction-affecting features. In the first identification step, the velocity and temperature effects under a no-load condition are examined to identify velocity- and temperature-dependent parameters. The second identification step considers the load effect at a constant temperature and velocity to identify load-dependent parameters. From the conducted experiments, the following observations are made:

- the quadratic character of the friction dependence on load
- the non-linear friction dependence on the velocity at some constant operating temperature
- the variation in load-dependent friction with velocity change

The dissipative property of the proposed friction model is analyzed, and the model parameters are constrained to guarantee the passivity of the model. The proposed friction model is evaluated in two robotic applications. In the first application, considering temperature and load dependency of friction resulted in a significant improvement in the root-mean-square errors up to 76% and 70% compared to uncompensated and compensated with standard friction model (22), respectively. In the second robotic application, the friction compensation factor, which depends on the friction model used, is increased from $\alpha_{fric} \approx 0.35$ to $\alpha_{fric} \approx 0.85$ since the friction model included the load and temperature effects. This resulted in a significant decrease in the interaction force up to 66% and ensured that the teaching force did not change with the variation in the robot's configuration and temperature. This paper's proposed friction model and estimation technique are valid for serial link collaborative industrial robots with serial kinematic structure and a modular joint containing strain-wave transmission.

In future studies, an online model parameter estimation algorithm will be developed to overcome time-consuming offline identifications. Furthermore, applications that benefit from the proposed model will be investigated.

REFERENCES

[1] W.-S. Huang, C.-W. Liu, P.-L. Hsu, and S.-S. Yeh, "Precision control and compensation of servomotors and machine tools via the disturbance observer," *IEEE Trans. Ind. Electron.*, vol. 57, no. 1, pp. 420–429, Jan. 2010.

[2] J. Wu, Z. Xiong, K.-M. Lee, and H. Ding, "High-acceleration precision point-to-point motion control with look-ahead properties," *IEEE Trans. Ind. Electron.*, vol. 58, no. 9, pp. 4343–4352, Sep. 2011.

[3] H. Chaoui and P. Sicard, "Adaptive fuzzy logic control of permanent magnet synchronous machines with nonlinear friction," *IEEE Trans. Ind. Electron.*, vol. 59, no. 2, pp. 1123–1133, Feb. 2012.

[4] M. Iwasaki, K. Seki, and Y. Maeda, "High-precision motion control techniques: A promising approach to improving motion performance," *IEEE Ind. Electron. Mag.*, vol. 6, no. 1, pp. 32–40, Mar. 2012.

[5] R. H. A. Hensen, *Controlled Mechanical Systems With Friction*. Technische Universiteit Eindhoven, 2002, doi: 10.6100/IR551394.

[6] A. Wahrburg, J. Bös, K. D. Listmann, F. Dai, B. Matthias, and H. Ding, "Motor-current-based estimation of Cartesian contact forces and torques for robotic manipulators and its application to force control," *IEEE Trans. Autom. Sci. Eng.*, vol. 15, no. 2, pp. 879–886, Apr. 2018.

[7] A. C. Bittencourt, "Modeling and diagnosis of friction and wear in industrial robots," Ph.D. dissertation, Linköping Univ. Electron. Press, Linköping, Sweden, 2014.

[8] E. Villagrossi, "Robot dynamics modelling and control for machining applications," Dipartimento di Engegneria Meccanica e Industriale, Università degli Studi di Brescia, Brescia, Italy, 2016.

[9] A. De Luca and L. Ferrajoli, "Exploiting robot redundancy in collision detection and reaction," in *Proc. IEEE/RSJ Int. Conf. Intell. Robots Syst.*, Sep. 2008, pp. 3299–3305.

[10] S. Goto, T. Usui, N. Kyura, and M. Nakamura, "Forcefree control with independent compensation for industrial articulated robot arms," *Control Eng. Pract.*, vol. 15, no. 6, pp. 627–638, Jun. 2007.
[11] A. C. Bittencourt, "Friction change detection in industrial robot arms," M.S. thesis, KTH Elect. Eng., Stockholm, Sweden, 2007.
[12] R. R. Waiboer, "Dynamic modelling, identification and simulation of industrial robots:–for off-line programming of robotised laser welding–," 2007.
[13] B. Armstrong-Helouvry, *Control of Machines With Friction*, vol. 128. Springer, 2012.
[14] P. R. Dahl, "A solid friction model," Aerosp. Corp., El Segundo, CA, USA, Tech. Rep. TOR-0158(3107-18)-1, 1968.
[15] C. C. de Wit, H. Olsson, K. J. Astrom, and P. Lischinsky, "A new model for control of systems with friction," *IEEE Trans. Autom. Control*, vol. 40, no. 3, pp. 419–425, Mar. 1995.
[16] V. Lampaert, J. Swevers, and F. Al-Bender, "Modification of the leuven integrated friction model structure," *IEEE Trans. Autom. Control*, vol. 47, no. 4, pp. 683–687, Apr. 2002.
[17] F. Al-Bender and J. Swevers, "Characterization of friction force dynamics," *IEEE Control Syst. Mag.*, vol. 28, no. 6, pp. 64–81, Nov. 2008.
[18] S.-D. Lee and J.-B. Song, "Sensorless collision detection based on friction model for a robot manipulator," *Int. J. Precis. Eng. Manuf.*, vol. 17, no. 1, pp. 11–17, Jan. 2016.
[19] A. Wahrburg, S. Klose, D. Clever, T. Groth, S. Moberg, J. Styrud, and H. Ding, "Modeling speed-, load-, and position-dependent friction effects in strain wave gears," in *Proc. IEEE Int. Conf. Robot. Automat. (ICRA)*, May 2018, pp. 2095–2102.
[20] L. Simoni, M. Beschi, G. Legnani, and A. Visioli, "On the inclusion of temperature in the friction model of industrial robots," *IFAC-PapersOnLine*, vol. 50, no. 1, pp. 3482–3487, Jul. 2017.
[21] T. Verstraten, G. Mathijssen, R. Furnémont, B. Vanderborght, and D. Lefeber, "Modeling and design of geared DC motors for energy efficiency: Comparison between theory and experiments," *Mechatronics*, vol. 30, pp. 198–213, Sep. 2015.
[22] P. Hamon, M. Gautier, and P. Garrec, "New dry friction model with load- and velocity-dependence and dynamic identification of multi-DOF robots," in *Proc. IEEE Int. Conf. Robot. Automat.*, May 2011, pp. 1077–1084.
[23] A. C. Bittencourt, E. Wernholt, S. Sander-Tavallaey, and T. Brogårdh, "An extended friction model to capture load and temperature effects in robot joints," in *Proc. IEEE/RSJ Int. Conf. Intell. Robots Syst.*, Oct. 2010, pp. 6161–6167.
[24] L. Gao, J. Yuan, and Y. Qian, "Torque control based direct teaching for industrial robot considering temperature-load effects on joint friction," *Ind. Robot, Int. J. Robot. Res. Appl.*, vol. 46, no. 5, pp. 699–710, Aug. 2019.
[25] E. Madsen, O. S. Rosenlund, D. Brandt, and X. Zhang, "Comprehensive modeling and identification of nonlinear joint dynamics for collaborative industrial robot manipulators," *Control Eng. Pract.*, vol. 101, Aug. 2020, Art. no. 104462.
[26] B. Armstrong-Hélouvry, P. Dupont, and C. C. De Wit, "A survey of models, analysis tools and compensation methods for the control of machines with friction," *Automatica*, vol. 30, no. 7, pp. 1083–1138, Jul. 1994.
[27] J. C. Willems, "Dissipative dynamical systems Part I: General theory," *Arch. Rational Mech. Anal.*, vol. 45, no. 5, pp. 321–351, 1972.
[28] H. Yu and P. J. Antsaklis, "Passivity and L_2 stability of networked dissipative systems," in *Proc. IEEE ICCA*, Jun. 2010, pp. 584–589.
[29] B. Bona and M. Indri, "Friction compensation in robotics: An overview," in *Proc. 44th IEEE Conf. Decis. Control, Eur. Control Conf. (CDC-ECC)*, Dec. 2005, pp. 4360–4367.
[30] W. Seyfferth, A. J. Maghzal, and J. Angeles, "Nonlinear modeling and parameter identification of harmonic drive robotic transmissions," in *Proc. IEEE Int. Conf. Robot. Automat.*, vol. 3, May 1995, pp. 3027–3032.
[31] A. Gogoussis and M. Donath, "Determining the effects of Coulomb friction on the dynamics of bearings and transmissions in robot mechanisms," *J. Mech. Des.*, vol. 115, no. 2, pp. 231–240, Jun. 1993.
[32] T. D. Tuttle and W. P. Seering, "A nonlinear model of a harmonic drive gear transmission," *IEEE Trans. Robot. Autom.*, vol. 12, no. 3, pp. 368–374, Jun. 1996.
[33] C. W. Kennedy and J. P. Desai, "Modeling and control of the mitsubishi PA-10 robot arm harmonic drive system," *IEEE/ASME Trans. Mechatronics*, vol. 10, no. 3, pp. 263–274, Jun. 2005.
[34] F. Altpeter, "Friction modeling, identification and compensation," EPFL, 1999.
[35] H. Olsson, "Control systems with friction," Ph.D. dissertation, Dept. Autom. Control, Lund Inst. Technol., 1996.
[36] Neuromeka. (2020). *Indy7 Robot*. [Online]. Available: https://www.neuromeka.com/
[37] C. C. de Wit and P. Lischinsky, "Adaptive friction compensation with partially known dynamic friction model," *Int. J. Adapt. Control Signal Process.*, vol. 11, no. 1, pp. 65–80, Feb. 1997.
[38] J. Park and W. Chung, "Design of a robust H∞ PID control for industrial manipulators," *J. Dyn. Syst., Meas., Control*, vol. 122, no. 4, pp. 803–812, Dec. 2000.

MESERET ABAYEBAS TADESE received the B.Sc. degree in electrical engineering from the Addis Ababa Institute of Technology, Ethiopia, in 2015, and the Ph.D. degree from the Robotics and Intelligent System Engineering Laboratory, Sugnkyunkwan University (SKKU), South Korea, in 2016. Before starting his Ph.D., he worked as an Assistant Lecturer with the Addis Ababa Institute of Technology. His research interest includes modeling, analysis, and nonlinear control theory with applications to mechatronic systems, including robot manipulators and others. He also works on physical human–robot interaction.

FRANCISCO YUMBLA (Student Member, IEEE) received the B.S. degree in electrical engineering from the Escuela Superior Politécnica del Litoral (ESPOL) with a focus on electronics and industrial automation. He is currently pursuing the Ph.D. degree in mechanical engineering with the Robotics and Intelligent Systems Engineering Laboratory, Sungkyunkwan University (SKKU). His research interests include combination task and motion planning, and dual-arm manipulation.

JUNE-SUP YI received the B.S. degree in mechanical engineering from Sungkyunkwan University, in 2016, where he is currently pursuing the Ph.D. degree with the Robotics and Intelligent Systems Engineering Laboratory. His research interests include assembly automation and task planning optimization.

WOONGYONG LEE received the B.S. degree in mechanical engineering from Sungkyunkwan University, Seoul, South Korea, in 2012, and the Ph.D. degree in mechanical engineering from the Robotics Laboratory, Pohang University of Science and Technology (POSTECH), Pohang, South Korea, in 2020. He is currently a Researcher with Nueromeka, a cooperative robot company, Seoul. His research interest includes the development and robust control of electric and electro-hydraulic systems, and their applications to the robotic systems.

JONGHOON PARK (Member, IEEE) received the B.S., M.S., and Ph.D. degrees in mechanical engineering from the Pohang University of Science and Technology (POSTECH), South Korea, in 1992, 1994, and 1999, respectively. He joined the Hiroshima University, Japan, as a Visiting Researcher, in 2000. In 2013, he founded Neuromeka, the first industrial collaborative robot (cobot) company in South Korea. He is currently the CEO of the company and an Adjunct Professor with the Department of Mechanical Engineering, POSTECH. His research interests include control of kinematically redundant manipulators, lie-group based robot analysis and control, nonlinear H-infinity optimal control of euler-lagrange systems, and task-based impedance control of robot manipulators.

HYUNGPIL MOON (Member, IEEE) received the B.S. and M.S. degrees in mechanical engineering from the Pohang University of Science and Technology, Pohang, South Korea, in 1996 and 1998, respectively, and the Ph.D. degree in mechanical engineering from the University of Michigan, Ann Arbor, MI, USA, in 2005. From 2006 to 2007, he was a Postdoctoral Researcher with the Robotics Institute, Carnegie Mellon University. In 2008, he joined the Faculty of the School of Mechanical Engineering, Sungkyunkwan University, Suwon, South Korea, where he is currently a Professor. His current research interests include robotic manipulation, SLAM, combined task and motion planning, and polymer-based sensor and actuators. He is also the Co-Chair for IEEE RAS TC on Robotic Hand, Grasping, and Manipulation. He was a Technical Editor of IEEE/ASME TRANSACTIONS MECHATRONICS, and the Editor-in-Chief of *Journal of Korea Robotics Society*. He is also serving as an Editor for *ICRA*, and an Associate Editor for *Intelligent Service Robotics*.